Fabrication of nano Ag encapsulated on ZnO/Fe2V4O13hybrid-heterojunction for photodecomposition of Methyl Orange

MUTHUVEL I (profmuthuvelchem@yahoo.com)
Annamalai University Faculty of Science https://orcid.org/0000-0002-0957-7688
K. Gowthami
B. Krishnakumar
C. Surya
G. Thirunarayanan
E. Vaishnavi

Research Article

Keywords: ZnO. Photodegradation. Ag-ZnO/Fe¬2¬V¬¬4¬O13. Methyl Orange. Nano-heterojunction. Wastewater treatment

Posted Date: February 25th, 2022

DOI: https://doi.org/10.21203/rs.3.rs-1359153/v1

Abstract

Novel Ag encapsulated nanocompositesZnO/$Fe_2V_4O_{13}$ (AZF) were synthesized with various wt% of the silver (from 1.0 to 2.5 wt% of Ag) by photo-deposition method using UV-A light. The nanostructure of the AZF was explored by various characterization techniques. Surface functional group was confirmed by FT-IR spectra, the crystalline nature of the material revealed by XRD patterns. Furthermore, surface morphology and optical properties of the composites were analyzed by SEM, HR-TEM UV-DRS and PL respectively. The photoactivity was tested against Methyl Orange (MO) degradation under UV light. The stability of the catalyst was confirmed by reusability measurements. Suitable degradation pathway was proposed based on intermediates obtained during degradation analyzed by GC-MS. Trapping experiments confirmed that super oxide radical anion ($O_2^{\cdot -}$) has been consider as a most active species for this degradation process. Mineralization is confirmed by measurements of chemical oxygen demand (COD).

1. Introduction

Dye pollutants released by the textile industries are becoming a significant source of pollution for the environment. It is estimated that about 150 tons a day will be released into the aquatic system worldwide.The discharge of this dye effluent is a major cause of non-esthetic degradation in the water body and these dyes are also resistant to aerobic degradation and can be converted into carcinogenic aromatic amines under anaerobic conditions [1–4]. Advanced oxidation processes (AOPs) producing hydroxyl radical ($^{\cdot}OH$) as one of the most effective oxidants were considered promising techniques. Photocatalytic processes based on the application of semiconductors as a photocatalyst for the degradation of toxic organic contaminants to in aqueous phase have been widely studied among various AOPs [5–9].In the photocatalytic activity of certain dye molecules, zinc oxide (ZnO) is documented to be more effective than TiO_2[10, 11]. ZnO is becoming a good choice for photocatalyst applications. ZnO is found to be inefficient alternative to TiO_2 since its photodegradation mechanism has been proved to be almost same. However, ZnO has a wide band gap of 3.37 eV, which ultimately limits in phtotodegradation due to rapid electron-hole recombination. Different attempts have been made to enhance the effective charge separation in ZnO to address this limitation, thus strengthening its photocatalytic ability. Encapsulation of noble metal nanocomposite has been proven efficacious due to strong surface plasma resonance (SPR) of noble metal which extendedvisible light absorption with charge separation. Recently, Nanosilver (AgNPs) has been paying intense attentiondue to its high performance of photocatalytic ability when it combined with semiconductors. Ag has been identified as the best elements to encapsulate with ZnO, due to its high solubility [12].

Recently photocatalysts based on Ag have been developed as effective photocatalysts for pollutant degradation [13, 14].Although both materials show great potential, due to recombination of the e^-/h^+ pair[15–17], they do not operate with high photocatalytic efficiency. The goal of this research work was to use the catalyst Ag-ZnO/$Fe_2V_4O_{13}$ to study the mineralization of MO dye by photodegradation using a technique different from the approaches mentioned above. The synthesized sample is characterized

using techniques such as FT-IR, XRD, BET, SEM-EDX, ECM, HR-TEM, UV-vis-DRS, and PL measurements. The photocatalytic properties of nanocomposites Ag-ZnO/$Fe_2V_4O_{13}$ (AZF) were assessed through the MO degradation under UV irradiation.

2. Experimental

2.1 Fabrication of Ag coated with ZnO/$Fe_2V_4O_{13}$

The synthesis of $Fe_2V_4O_{13}$ and $Fe_2V_4O_{13}$/ZnO was reported in our previous paper [18, 19]. Different concentrations of Ag^+ ions were added into the suspension (C_2H_5OH/H_2O as solvent) of 3 g of synthesized $Fe_2V_4O_{13}$/ZnO such that the Ag^+ concentration was (X wt%; where X = 1, 1.5, 2, 2.5) in relation to $Fe_2V_4O_{13}$/ZnO. The mixed suspensions were placed in photoreactor then irradiated for 3 h with 8×8W mercury lamps UV-A light under continuous stirring.During irradiation Ag^+ converted into Ag and deposited on ZnO/$Fe_2V_4O_{13}$nanocomposite (AZF). The AZF were centrifuged and dried at 100 °C for 2 h then used as photocatalyst. The chemicals used for this study, instrumental specification for the characterization techniques, the photocatalytic experimental and COD measurements procedures are given in supporting information's. The photoreactor used for this study is given as Fig. S1 (see Supporting information).

3. Results And Discussion

3.1 FT-IR

Figure 1 shows FT-IR spectra of prepared ZnO, $Fe_2V_4O_{13}$, and X-AZF (X = 1, 1.5,2 and 2.5 wt%). The stretching vibration of surface hydroxyl group was appeared in the range between 3453 and 3405 cm^{-1} for all the samples[18, 19]. In Fig. 1a, peaks observed at 420, 447, and 543 cm^{-1}, which could be attributed to the Zn–O stretching modes [19–21].In Fig. 1b, the peaks at 1028,711 and 510 cm^{-1} are assigned to V–O, V–O–Fe and Fe–O stretching modes, respectively[19].Bands at 474 and 426 $cm^{-1}$are attributed to the characteristic stretching mode of Ag–O and Zn–O bonds[22]. Figure 1c–f show various functional groups of AZF and the metal oxide bond present in the compound, Fe–O, Ag–O, and Zn–O vibrations are observed at 1015, 1100, 474, 426, and 413 cm^{-1}. This indicates that Ag was effectively loaded on the ZnO/$Fe_2V_4O_{13}$ nanocomposite.

3.2 XRD

Figure 2 show the typical X-ray diffraction (XRD) patterns of the prepared ZnO(Fig. 2a),$Fe_2V_4O_{13}$ (Fig. 2b) [19] and ZnO/$Fe_2V_4O_{13}$ samples with different loading concentrations of Ag (X = 1, 1.5, 2 and 2.5 wt%) (Fig. 2c–f). The wurtzite ZnO (JCPDS Card No. 36-1451) planes were observed for the prepared ZnO at 2θ values of 31.75, 34.40, 36.23, 47.53, 56.60, and 62.34° corresponds to (100), (002), (101), (102), (110), and (103) planes, respectively[23, 24].In Fig. 2b, $Fe_2V_4O_{13}$ shows three diffraction peaks at 2θ angles of

12.5, 22.7, and 26.7° that correspond to (002), (022), and (014) planes of $Fe_2V_4O_{13}$, respectively and the peaks are well matched to the monoclinic phase of $Fe_2V_4O_{13}$ (JCPDS Card No. 00-039-0893). The good crystallinity is confirmed by high and narrow diffracted peaks[19]. Face centered cubic (FCC) geometry is indexed to the three additional peaks at 38.06, 44.29, and 64.43° corresponding to (111), (200), and (220) planes of ZnO/$Fe_2V_4O_{13}$ doped with silver nanocomposites (JCPDS Card No. 4-0783)[25, 26] inFig. 2c–f. The average crystallite size of 2 wt% of AZF was 28.5 nm.

3.3 BET surface area

The pore structure and surface area of the prepared Ag-ZnO/$Fe_2V_4O_{13}$ was analyzed using N_2 absorption-desorption isotherms are shown in Fig. 3. The Ag-ZnO/$Fe_2V_4O_{13}$ is type II isotherm at IUPAC level[27]and the distribution of pore size is given in the inset of Fig. 3. The BET surface area and pore volume of Ag-ZnO/$Fe_2V_4O_{13}$ are given in Table 1.

Table 1
Texture parameters of 2 wt% Ag-ZnO/$Fe_2V_4O_{13}$

S_{BET} ($m^2\ g^{-1}$)	V_p ($cm^3\ g^{-1}$)	D_p (nm)	S_{micro} ($m^2\ g^{-1}$)	V_{micro} ($cm^3\ g^{-1}$)
0.9043	0.1044	461.86	16.53	0.0089

S_{BET} = BET surface area, V_p = total pore volume, D_p = average uniform pore size distribution, S_{micro} = surface area of micropores, V_{micro} = pore volume of micropores.

Table 2
Mass spectral data of intermediates (MO)

Compounds	Retention time (min)	m/z values
$C_{13}H_{13}N_3O_3S$ (**D1**)	19.796	292.0 (M + 1), 258.0, 229.0, 181.0, 152.0, 126.0, 111.0, 75.0
$C_{12}H_9N_2NaO_3S$ (**D2**)	18.533	284.0 (M^+), 282.0, 211.0, 111.0, 85.0, 71.0, 57.0, 54.0
$C_6H_5N_2NaO_3S$ (**D3**)	16.665	209.0 (M^+), 111.0, 97.0, 85.0, 71.0, 57.0
C_6H_7NO (**D4**)	15.512	109.0 (M^+), 83.0, 71.0, 67.0, 57.0

3.4 SEM-EDX with color mapping

SEM measurements have described the surface morphology of the AZF. Figure 4shows that the 2 wt% Ag-loaded ZnO/$Fe_2V_4O_{13}$ with different magnifications. The irregular-shaped ZnO/$Fe_2V_4O_{13}$ agglomerates are shown in all SEM images.EDX can generally accurately detect up to trace amount of metal present on the surface of base materials. Figure 5 shows the EDX recorded from the selected area, which reveals that

the presence of Zn, Fe, V, Ag, and O in the catalyst. The presence of these elements in Ag-ZnO/$Fe_2V_4O_{13}$ was also confirmed by elemental color mapping. The different color areas in Fig. 6 indicate Ag, Zn, Fe, V, and O enriched areas of the Ag-ZnO/$Fe_2V_4O_{13}$ sample.

3.5 HR-TEM

Figure 7shows that the HR-TEM images of the 2 wt% Ag-ZnO/$Fe_2V_4O_{13}$.From Fig. 7a, some of the hexagonal particles are clearly seen, and corresponding to ZnO in Ag-ZnO/$Fe_2V_4O_{13}$, although the identification of $Fe_2V_4O_{13}$ in Ag-ZnO/$Fe_2V_4O_{13}$ was impossible. The lattice fringes of the Ag-ZnO/$Fe_2V_4O_{13}$ catalyst are shown inFig. 7d. The interplanar spacing values for the nanocrystalline Ag-ZnO are shown in Fig. 7e. From the HR-TEM images, the average diameters (28.545±5.453nm) of the nanoparticles (Ag-ZnO/$Fe_2V_4O_{13}$nanocomposite) were computed by Image J analysis. The histogram shows that the average particle diameter of 2wt% Ag-ZnO/$Fe_2V_4O_{13}$in Fig. 7f.

3.6 UV-vis-DRS

Figure 8Ashows the DRS results of ZnO, $Fe_2V_4O_{13}$, and samples with various wt % of X-Ag-loaded ZnO/$Fe_2V_4O_{13}$ (X = 1.0, 1.5, 2 and 2.5 wt%) catalyst. In visible regions, Ag-ZnO/$Fe_2V_4O_{13}$ composites display higher absorption than ZnO, resulting in higher visible light active catalytic behavior and also an increase in the absorption at 350–380 nm (UV-region) this can contribute to enhanced e^-/h^+pair production, which consequently improvesthe photocatalyticactivity under UV light[28]. Figure 8B shows K-Mplots for ZnO, $Fe_2V_4O_{13}$, and ZnO/$Fe_2V_4O_{13}$ with various wt % of Ag loading. The band gap energies of ZnO, $Fe_2V_4O_{13}$, and X-Ag-ZnO/$Fe_2V_4O_{13}$ (X = 1, 1.5, 2, and 2.5 wt%) were 3.25, 2.21, 3.23, 3.23, 3.15, and 3.16 eV, respectively.

3.7 Photoluminescence (PL) emission spectra

The effective suppression of photogenerated charge carriers and the transfer of the photogenerated e^-/h^+were investigated by photoluminescence (PL) emission spectra[29]. Figure 9 shows the PL spectra of the prepared ZnO (Fig. 9a) and 2 wt% Ag-ZnO/$Fe_2V_4O_{13}$ (Fig. 9b). Three emission bands are observed at 395, 431, and 586 nm. Although all the peaks are almost identical, PL intensities are different. The higher intensitywas observed in bare ZnO at 395 nm due to high e^-/h^+recombination than Ag-ZnO/$Fe_2V_4O_{13}$. The Ag particles loaded with the ZnO/$Fe_2V_4O_{13}$nanocompositeact as trapper for photo-generatedelectrons, and quench the PL emission [30].The maximum intensity shows the higher e^-/h^+ recombination and resultslow photocatalytic activity[31, 32].The lowest intensity shows that the well suppression of e^-/h^+recombination and results higher photocatalytic activity[33].

3.8 Primary analysis

The photocatalytic behavior of nanocomposite Ag-ZnO/$Fe_2V_4O_{13}$ with 1, 1.5, 2, and 2.5 wt percent of Ag loading was assessed in terms of MO degradation.Controlledexperimentswere conducted under different reaction conditions (Fig. 10). The dye/ZnO/UV-A process underwent 68% degradation in 90 min (curve a).

The dye/ZnO/$Fe_2V_4O_{13}$/UV light process showed curve b, which yielded 75% degradation in 90 min. Only 19% adsorption was observed in dye/2 wt% Ag-ZnO/$Fe_2V_4O_{13}$/dark process (curve e).Curves c, d, f, and g demonstrate the degradation of dye on irradiation with the Ag-ZnO/$Fe_2V_4O_{13}$ catalyst with different percent wt of Ag loading. The 2 wt% Ag-ZnO/$Fe_2V_4O_{13}$hybrid-heterojunction catalyst showed higher MOdegradation (curve f, 93%) in 90 min and also almost complete degradation was achieved at 120 min. Hence, 2 wt% of Ag is the optimum loading of Ag-ZnO/$Fe_2V_4O_{13}$.

3.9 Effect of pH

pH is the important parameters for the application of industrial point of view.By adjusting the pH of the MO solution, the effect of pH on the MO photodegradation was studied. Fig. S2demonstrates that pH has an important effect on the rate of photodegradation and decolorization. The maximum degradation and decolorization of MO is observed at pH 7. Above pH 7, the rate of degradation and decolorization decreases. Effect of catalyst loading (Fig. S3) and initial dye concentration (Fig. S4) are discussed in supporting information's.

3.10 Reusability

Figure 11 shows the stability of the catalyst for the degradation of MO. In the first run, approximately 99% of MO degradation achieved. The same catalyst was again reused for further runs. All the remaining cycles gave almost 98.5% of degradation in 90 min. Hence, the 2 wt% Ag-ZnO/$Fe_2V_4O_{13}$ is stable, recoverable and reusable.

3.11 Mineralization studies

3.11.1 GC-MS analysis

Sometimes intermediates are more hazardous than starting materials, so it is necessary to analyze the intermediates for the degradation process. An attempt has been made to find out the degradation intermediates of MO photodegradation with 2wt% Ag-ZnO/$Fe_2V_4O_{13}$ (AZF) hybrid-heterojunction/UV process. GC-MS studied performed with the solutions obtained after 30 and 60 minutes of irradiation and predicted a degradation pathway for MO by AZF based on the m/z ratio, retention time and molecular weight(Scheme 1). For these identified intermediates, molecular ion and fragmentation peak values are stated inTable 2.Although, in photocatalytic degradation of azo dyes, it was expected that the cleavage of azo bond take place first, however, formation of compounds observed (**D1** and **D2**)with azo groups at the retention time of 19.796 and 18.533 min, respectively. Hydroxyl radicals were thus considered to be the most reactive species for degradation, the compound **D1** undergoes azo link cleavage and replacement of sulfonic acid group by hydroxyl group through the repetitive attack of ˙OH radicals produced intermediates *N*-methylbenzene-1,4-diamine (Compound **I**) and 4-aminophenol (**D4**). The intermediate product **D2** further undergoes C–N cleavage produced **D3** which on further undergoes azo link cleavage produced 4-aminophenol (**D4**). Finally, it is expected that the compound **D4** and compound **I** would be mineralized to CO_2, water and mineral acids [34, 35].

3.11.2 FT-IR spectral analysis

The early adsorption of the dye under dark by 2 wt% Ag-ZnO/$Fe_2V_4O_{13}$nanocomposite is 33.4%, although complete degradation occurred at 90 min irradiation. The experiments were carried out to determine whether the adsorbed dye molecules had been degraded completely. Comparisons made with FT-IR spectra of the fresh dye and catalyst ((Fig. S5a and S5b), and dye adsorbed composite before and after irradiations (Fig. S5c and S5d). The characteristic bands of MO (Fig. S5a) are observed at 1604, 1366, and 1042 cm^{-1} due to N = N stretching, C–N bond vibrations, and S = O bond of MO, respectively [36].When compared Fig. S5a and Fig. S5c, the characteristic MO dye peaks are observed in the dye adsorbed catalyst. However, upon irradiation,*ie* after complete degradation, the FT-IR spectrum of the composite (Fig. S5d) resembles with fresh catalyst (Fig. S5b) revealed that the adsorbed dye molecules underwent complete degradation.Thus, the 2 wt% Ag-ZnO/$Fe_2V_4O_{13}$nanocomposite shows better catalytic performance for MO.

3.11.3 UV-Vis spectral analysis

Figure 12 shows UV-vis spectra for the degradation and decolorization of MO by 2 wt% Ag-ZnO/$Fe_2V_4O_{13}$nanocomposite under UV-A light irradiation for 0–90 min. UV-vis spectrum of MO shows strong absorption in the range of 200–600 nm with λ_{max} at 464 nm, which is due to the presence of the azo group (N = N), and another band is observed at 272 nm in the UV region due to aromatic part of the dye. Upon continues irradiation with2 wt% Ag-ZnO/$Fe_2V_4O_{13}$nanocomposite, both peaks were diminished with respect to time, and finally almost completely disappeared. From these observations we conclude that the degradation of the dye with respect to time[37].Moreover, no new peakswere observed during irradiation, indicating that MO was degraded gradually and intermediates do not absorb at analytical wavelengths. The color of the suspension changed from the orange to colorless (inset of Fig. 12).

3.11.4 Chemical oxygen demand (COD) measurements

The mineralization of the dye further confirmed with reduction of COD values. Under optimum condition, COD measurements were made and the percentageof COD reduction of thedye at different times of UV-A light irradiation is given in Table 3. Percentages of COD reduction increases with respect to irradiation time reveals that the mineralization of the dye.

Table 3
Percentages of COD reduction at different irradiation times for the degradation of MO by 2 wt% Ag-ZnO/$Fe_2V_4O_{13}$ catalyst

Dye	0 min	30 min	60 min	90 min	120 min
MO	0	31.6	57.4	79.3	88.0

[MO] = $4 \cdot 10^{-4}$ M, 2 wt% Ag-ZnO/$Fe_2V_4O_{13}$ = 3 g L^{-1}, airflow rate = 8.1 mL s^{-1}, pH = 7, I_{UV} = $1.381 \cdot 10^{-6}$ einstein L^{-1} s^{-1}.

3.12 Mechanism

Under light irradiation, the photoexcited electrons in the CB of $Fe_2V_4O_{13}$ can jump to the CB of ZnO. The CB potential of ZnO was found to be more electronegative than the reduction potential of $O_2/O_2^{\bullet-}$ (−0.34 eV *vs* NHE), and therefore, the electrons concentrated in the CB of ZnO can generate $O_2^{\bullet-}$ for dye degradation(Fig. 13). Further, Ag can shuttle the photogenerated electron from ZnO in Ag-ZnO/$Fe_2V_4O_{13}$ and reduces the recombination of electron-hole pair effectively. However, owing to the less positive VB potential of $Fe_2V_4O_{13}$, the holes do not generate $^{\bullet}$OH. Meanwhile, $Fe_2V_4O_{13}$'s holes created in the VB would be transferred to its surface and then directly involved in the MO degradation.By these two processes the lifetimes of electron and hole increase, leading to enhanced photocatalytic activity.

The increased transfer of charge between the interface of $Fe_2V_4O_{13}$ and ZnO strongly suppressed the rate of recombination, which is beneficial to improve the photocatalyticability. The reduction of PL intensity in Ag-ZnO/$Fe_2V_4O_{13}$ as compared to that of pure undopedZnOreveals the effective prohibition of recombination of e^-/h^+pairs, indicating thatloadingof Ag and $Fe_2V_4O_{13}$ could substantiallysuppress the charge transfer rate in ZnO. The band gap energy of Ag-ZnO/$Fe_2V_4O_{13}$lowered than that of pure ZnO.

In general, for a higher formation rate of $^{\bullet}$OH radicals, a separation efficiency of electron-hole pairs would be greater. The photocatalytic activity therefore shows a positive association with the rate of radical formation of $^{\bullet}$OH, i.e., a faster rate of radical formation of •OH contributes to a higher photocatalytic activity of the nanocomposite. Moreover, the formation of superoxide radical anions increased due to electrons transferred to the adsorbed oxygen molecules by Ag *via* the ZnO conduction band. Hydroxyl radicals and superoxide radical anions are potent oxidants, so that organic molecules and intermediate species can completely oxidizedtotheir respective end-products.

Trapping experiments were performed to identify the active species involved in photocatalytic degradation process[38–40] and the results are shown in Fig. 14. No scavenger, the degradation efficiency is 99% at time of 90 min. Under the same condition, with TBA ($^{\bullet}$OH scavenger), KI (h^+ scavenger), BQ ($O_2^{\bullet-}$ scavenger) and $AgNO_3$ (e^- scavenger) gave 93.9, 86.8, 84.6 and 89.6 percentages of degradation, respectively. From these values, more or less all the species are equally contributed in the degradation process. However, the addition of BQ suppress the photocatalytic activity of the composite insomewhat extent, hence superoxide radical anion ($O_2^{\bullet-}$) has been consider as a most active species for this degradation process.

4. Conclusions

Ag loaded ZnO/$Fe_2V_4O_{13}$nanocomposites have been prepared using photo-deposition method. The prepared nanocomposite was characterized by various technique. The photocatalytic activities of Ag-ZnO/$Fe_2V_4O_{13}$nanocomposite were evaluated using degradation of MO under UV-A light irradiation, and almost complete degradation was observed with 2 wt% Ag loaded $Fe_2V_4O_{13}$/ZnO composite. The neutral pH (7) facilitate the degradation efficiently with3 g L^{-1} catalyst loading. The stability of the catalyst was

observed by multiple runs of the catalyst. Almost 99% of degradation was observed for all the five runs. GC-MS reveals that the formation of three azo compounds (**D1**, **D2** and **D3**) and 4-aminophneol (**D4**) as intermediates during degradation process. Trapping experiments confirms that the super oxide radical anion ($O_2^{\bullet -}$) has been considered as a most active species for this degradation process. The complete mineralization was confirmed by COD measurement. A suitable degradation mechanism is also proposed.

Declarations

Conflicts of interest

There is no conflict of interest declare

Acknowledgements

The authors (Dr. IM) thanks University Grants Commission (UGC), New Delhi for the financial support (F.No-43-222/2014(SR)).Dr. B.K thanks award from Yonsei Frontier Program for Young Postdoctoral Researchers 2020, Yonsei University, Seoul, Korea. I would like to thank DST-SAIF Cochin,Cochin University of Science &Technology Campus, Kochi 682 022, Kerala, India for taking HR-TEM analysis.

Electronic supplementary information (ESI)

Figs. S1–S5, the chemicals used for this study, instrumental specification for the characterization techniques, the photocatalytic experimental and COD measurements procedures are given in supporting information's.

References

1. P.B. Koli, K.H. Kapadnis, U.G. Deshpande, M.R.Patil,Fabrication and characterization of pure and modified Co_3O_4 nanocatalyst and their application for photocatalytic degradation of eosin blue dye: a comparative study. J. nanostructure chem. **8**, 453–463 (2018)
2. A. Phuruangrat, P.O. Keereesaensuk, K. Karthik, P. Dumrongrojthanath, N. Ekthammathat, S. Thongtem, T.Thongtem, Synthesis of Ag/Bi_2MoO_6 Nanocomposites Using $NaBH_4$ as Reducing Agent for Enhanced Visible-Light-Driven Photocatalysis of Rhodamine B,J. Inorg. Organomet. Polym. Mater. **30**, 322–329 (2020)
3. S. Rajasri, B. Krishnakumar, A.J.F.N. Sobral, S. Balachandran, M. Swaminathan, I. Muthuvel, Development of $Cd_3(PO_4)_2$/rGOcoupled semiconductor system for effective mineralization of Basic Violet 10 (BV 10) under UV-A light, Mater. Today Proc.**15**,471–480(2019)
4. K.Tanka, K.Padermpole,T.Hisanaga,Photocatalytic degradation of commercial azodyes. Water Res. **34**, 327–333 (2000)

5. I. Muthuvel, M. Swaminathan, Photoassisted Fenton mineralisation of Acid Violet 7 by heterogeneous Fe(III)-Al_2O_3 catalyst. Catal. Commun. **8**, 981–986 (2007)
6. I. Muthuvel, M. Swaminathan, Highly solar active Fe(III) immobilized –Alumina for the degradation of Acid Violet 7. Sol. Energy Mater. Sol. Cells. **92**, 857–863 (2008)
7. M. Shirzad-Siboni, M.T. Samadi, J.K. Yang, S.M. Lee, Photocatalytic reduction of Cr(VI) and Ni(II) in aqueous solution by synthesized nanoparticle ZnO under ultraviolet light irradiation: a kinetic study. Environ. Technol. **32**, 1573–1579 (2011)
8. A. Rezaee, H. Masoumbeigi, R.D.C. Soltani, A. R. Khatee, S. Hashemiyan Photocatalyticdecolorization of methylene, blue using immobilized ZnO nanoparticles prepared by solution combustion method. Desalin. Water Treat. **44**, 174–179 (2012)
9. N. Zhang, Y. Zhang, Y.J. Xu, Recent progress on graphene-based photocatalysts: current status and future perspectives, Nanoscale. 4,5792–5813 (2012)
10. H.J. Lee, H. Kim, S.S. Park, S.S. Hong, G. D. Lee, Degradation kinetics for photocatalytic reaction of, methyl orange over Al-doped ZnO nanoparticles. J. Ind. Eng. Chem. **25**, 199–206 (2015)
11. S.A. Ansari, M.M. Khan, M.O. Ansari, J. Lee, M. H. Cho, Biogenic synthesis photocatalytic, and photoelectrochemical performance of Ag–ZnOnanocomposite. J. Phys. Chem. **117**, 27023–27030 (2013)
12. J. Yu, D. Sun, T. Wang, F. Li, Fabrication of Ag@AgCl/ZnO submicron wire film catalyst on glass substrate with excellent visible light photocatalytic activity and reusability.Chem. Eng. J. **334**, 225–236 (2018)
13. F.S. Hashim, A.F. Alkaim, S.J. Salim, A.H.O. Alkhayatt, Effect of (Ag, Pd) doping on structural, and optical properties of ZnOnanoparticales: As a model of photocatalytic activity for water pollution treatment. Chem. Phys. Lett. **737**, 136828 (2019)
14. M.J. Sampaio, M.J. Lima, D.L. Baptista, A.M.T. Silva, C.G. Silva, J.L. Faria, Ag-loaded ZnO materials for photocatalytic water treatment. Chem. Eng. J. **318**, 95–102 (2017)
15. F. Zhang, Y.H. Li, M.Y. Qi, Z.R. Tang, Y.J. Xu, Boosting the activity and stability of Ag-Cu_2O/ZnOnanorods for photocatalytic CO_2 reduction. Appl. Catal. B **.268**, 118380 (2020)
16. M. Ahmad, I. Ahmad, E. Ahmed, M.S. Akhtar, N.R. Khalid, Facile and inexpensive synthesis of Ag doped ZnO/CNTs composite: Study on the efficient photocatalytic activity and photocatalytic mechanism. J. Mol. Liq **311**, 113326 (2020)
17. M. Moradi, M. Haghighi, S. Allahyari, Precipitation dispersion of Ag–ZnOnanocatalyst,over functionalized multiwall carbon nanotube used in degradation of Acid Orange from wastewater,ProcessSafe. Environ. Prot. **107**, 414–427 (2017)
18. I. Muthuvel, K. Gowthami, G. Thirunarayanan, P. Suppuraj, B. Krishnakumar, A.J.F.N. Sobral, M. Swaminathan, Graphene oxide–$Fe_2V_4O_{13}$ hybrid material as highly efficient hetero-Fenton catalyst for degradation of methyl orange. Int. J. Ind. Chem. **10**, 77–87 (2019)

19. K. Gowthami, B. Krishnakumar, A.J.F.N. Sobral, G. Thirunarayanan, M. Swaminathan, R. Siranjeevi, T. Rajachandrasekar, I. Muthuvel, Fabrication of Hybrid $Fe_2V_4O_{13}$/ZnOHeterostructure for Effective Mineralization of Aqueous Methyl Orange Solution. J. Cluster Sci. **31**, 839–849 (2020)
20. K. Gowthami, P. Suppuraj, G. Thirunarayanan, B. Krishnakumar, A. J. F. N. Sobral M. Swaminathan, I. Muthuvel, $Fe_2V_4O_{13}$ assisted hetero-Fenton mineralization of methyl orange under UV-A light irradiation. Iran. Chem Commun **6**, 97–108 (2018)
21. B. Babu, T. Aswani, G.Thirumala Rao, R. Joyce Stella, B. Jayaraja, R.V.S.S.N. Ravikumar, Room temperature ferromagnetism and optical properties of Cu^{2+} doped ZnOnanopowder by ultrasound assisted solid state reaction technique. J. Magn. Magn. Mater. **355**, 76–80 (2014)
22. A.H. Shah, E. Manikandan, M. Basheer Ahmed, V.Ganesan, Enhanced Bioactivity of Ag/ZnONanorods-A Comparative Antibacterial Study. J. Nanomed. Nanotechnol **4**, 1000168 (2013)
23. G. Bandekar, N.S. Rajurkar, I.S. Mulla, U.P. Mulik, D.P. Amalnerkar, P. V. Adhyapak, Synthesis, characterization and photocatalytic activity of PVP stabilized ZnOand modified ZnO nanostructures. Appl. Nanosci. **4**, 199–208 (2014)
24. K. Rekha, M. Nirmala, G. Manjula, N.A. Anukaliani, Structural, optical, photocatalytic and antibacterial activity of zinc oxide and manganese doped zinc oxide nanoparticles. Phys. B **405**, 3180–3185 (2010)
25. S. Mohammadzadeh, M.E. Olya, A.M. Arabi, A. Shariati, M.R.K. Nikou, Synthesis, characterization and application of ZnO-Ag as a nanophotocatalyst for organic compounds degradation, mechanism and economic study. J. Environ. Sci. **35**, 194–207 (2015)
26. X. Yin, W. Que, D. Fei, F. Shen, Q. Guo, Ag nanoparticle/ZnOnanorodsnanocomposites derived by a seed-mediated method and their photocatalytic properties. J. Alloys Compd. **524**, 13–21 (2012)
27. Z. Qiu, D. He, Y. Wang, X. Zhao, W. Zhao, H. Wu, High performance asymmetric supercapacitors with ultrahigh, energy density based on hierarchical carbon nanotubes@NiO core–shell nanosheets and defect-introduced graphene sheets with hole structure. RSC Adv. **7**, 7843–7856 (2017)
28. M. Zheng, J. Wu, One-step synthesis of nitrogen-doped ZnOnanocrystallites and their properties. Appl. Surf. Sci. **255**, 5656–5661 (2009)
29. E.S. Baeissa, Photocatalytic degradation of methylene blue dye under visible light irradiation using In/ZnOnanocomposite,Front. Nanosci. Nanotechnol **2**, 1–5 (2016)
30. P. Suppuraj, K. Thirumalai, S. Parthiban, M. Swaminathan, I. Muthuvel, Novel Ag-TiO_2, /$ZnFe_2O_4$Nanocomposites for Effective Photocatalytic, Electrocatalytic and CytotoxicityApplications. J. Nanosci. Nanotechnol **20**, 709–718 (2020)
31. Q. Wang, J. Hui, J. Li, Y. Cai, S. Yin, F. Wang, B. Su, Photodegradationofmethyl orange with PANI-modified BiOClphotocatalyst under visible light irradiation. Appl. Surf. Sci. **283**, 577–583 (2013)
32. L. Ge, C. Han, J. Liu, *In situ* synthesis and enhanced visible light photocatalytic activities of novel PANI–g-C_3N_4 composite photocatalysts,J. Mater. Chem., **22**,11843–11850(2012)

33. H.A. Ghaly, A.S. El-Kalliny, T.A. Gad-Allah, N.E.A. Abd El-Sattar, E.R. Souaya, Stable plasmonic Ag/AgCl–polyaniline photoactive composite for degradation of organic contaminants under solar light. RSC Adv. **7**, 12726–12736 (2017)
34. B. Krishnakumar, B. Subash, M. Swaminathan, AgBr–ZnO–An efficient nano- photocatalyst for the mineralization of Acid Black 1 with UV light. Sep. Purif. Technol. **85**, 35–44 (2012)
35. S.Ravikumar,D. Mani, M.R. Khan, N.Ahmad,S.Sylvestre,C. Surya, B. Krishnakumar, V. Pandiyan, Y.H.Ahn,Ag-TiO_2@Pd/C nanocomposites for efficient degradation of Reactive Red 120 dye and ofloxacin antibiotic under UV and solar light and its antimicrobial activity,J. Environ. Chem. Eng. **9**(6), 106657 (2021)
36. D.C. Kalyani, A.A. Telke, S.P. Govindwar, J.P.Jadhav, Biodegradation and detoxification of reactive textile dye by isolated Pseudomonas sp. SUK1. Water Environ. Res. **81**, 298–307 (2009)
37. J. Deng, J. Jiang, Y. Zhang, X. Lin, C. Du,Y. Xiong,Hybrid copper doped titania/polythiophenenanorods as, efficient visible light-driven photocatalyst for degradation of organic pollutants. Appl. Catal. B **.84**, 468–473 (2009)
38. H. Liu, Y. Hu, Z. Zhang, X. Liu, H. Jia, B. Xu, Synthesis of spherical Ag/ZnOheterostructural composites with excellent photocatalytic activity under visible light and UV irradiation. Appl. Surf. Sci. **355**, 644–652 (2015)
39. H. Liu, H. Zhai, C. Hu, J. Yang, Z. Liu, Hydrothermal synthesis of In_2O_3 nanoparticles hybrid twins hexagonal disk ZnO heterostructures for enhanced photocatalytic activities and stability. Nanoscale Res. Lett. **12**, 466–477 (2017)
40. S. Rajasri, S.Kalikeri,S.Balachandran,K. Gowthami, G. Thirunarayanan, M. Swaminathan, I. Muthuvel, Enhanced photodegradation of 2,4-dinitrophenol by n–p type TiO_2/ BiOI nanocomposite. J. Indian Chem. Soc. **99**, 100337 (2022)

Scheme

Scheme 1 is available in supplementary section.

Figures

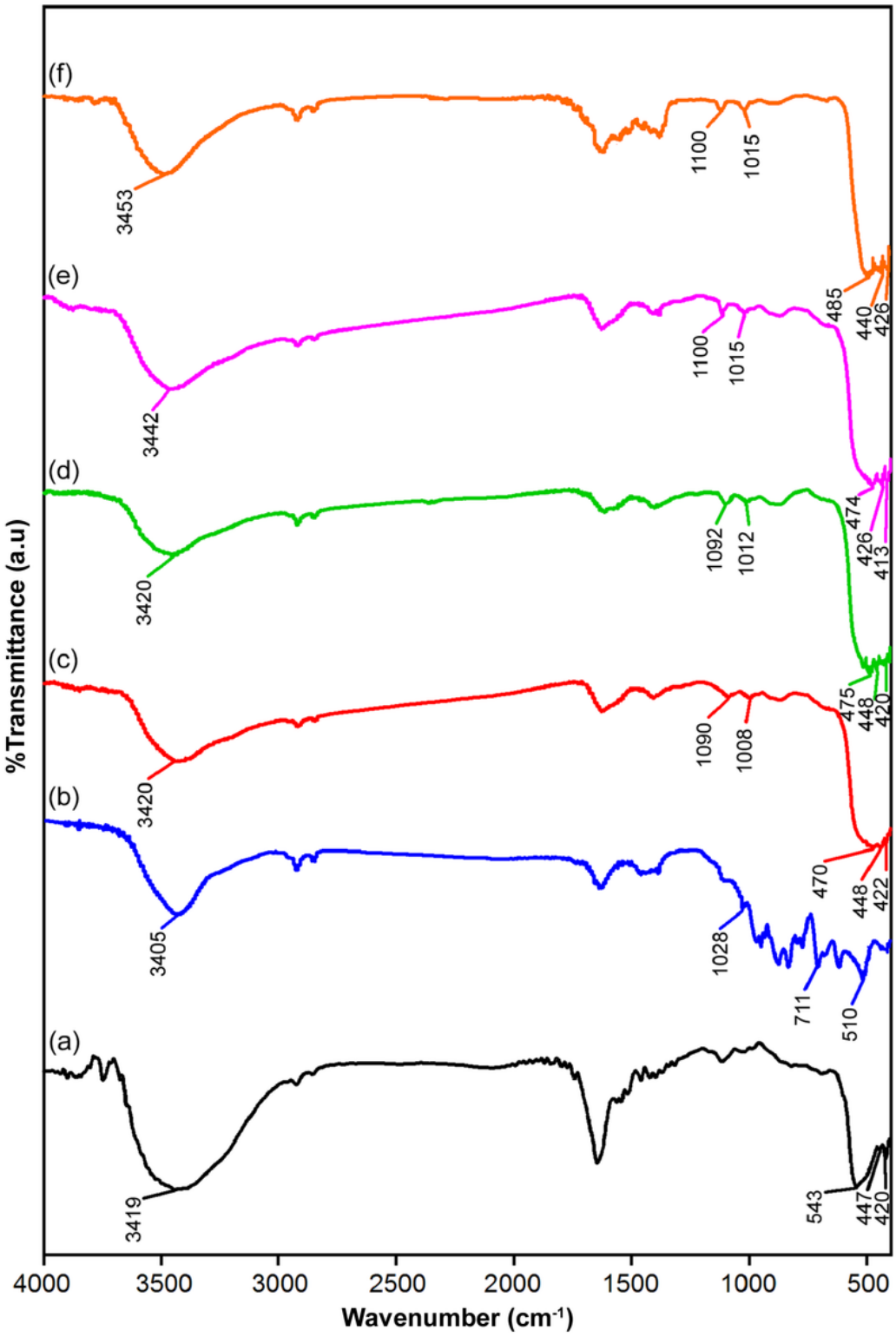

Figure 1

FT-IR spectra of a) ZnO, b) $Fe_2V_4O_{13}$, c) 1 wt% Ag-ZnO/$Fe_2V_4O_{13}$, d) 1.5 wt% Ag-ZnO/$Fe_2V_4O_{13}$, e) 2 wt% Ag-ZnO/$Fe_2V_4O_{13}$ and f) 2.5 wt% Ag-ZnO/$Fe_2V_4O_{13}$.

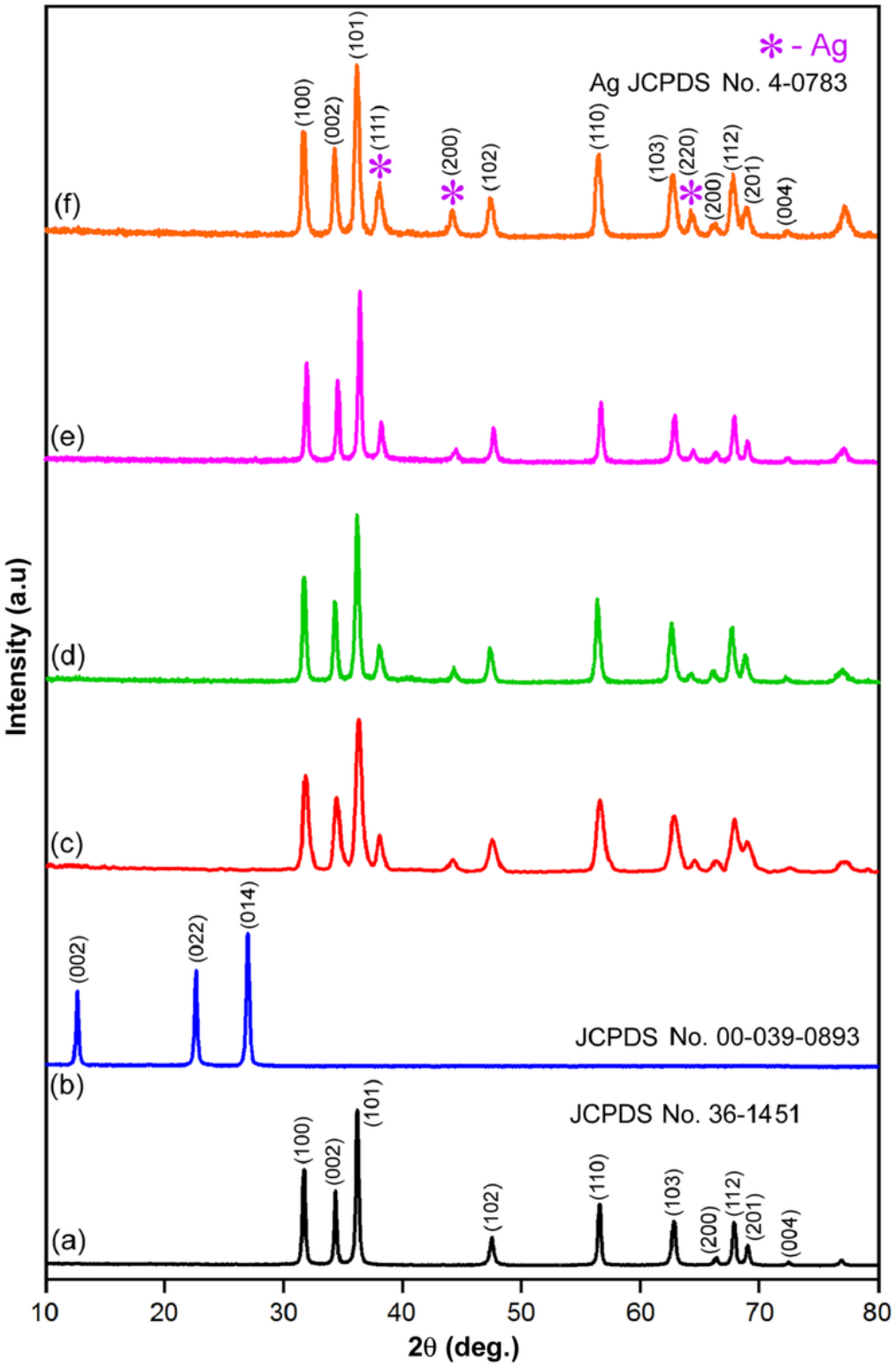

Figure 2

XRD patterns of a) ZnO, b) $Fe_2V_4O_{13}$, c) 1 wt% Ag-ZnO/$Fe_2V_4O_{13}$, d) 1.5 wt% Ag-ZnO/$Fe_2V_4O_{13}$, e) 2 wt% Ag-ZnO/$Fe_2V_4O_{13}$ and f) 2.5 wt% Ag-ZnO/$Fe_2V_4O_{13}$.

Figure 3

N_2 adsorption-desorption isotherm of 2 wt% Ag-ZnO/$Fe_2V_4O_{13}$. Inset shows pore size distribution.

Figure 4

SEM images of 2 wt% Ag-ZnO/$Fe_2V_4O_{13}$: a, b) 1 mm and c, d) 200 nm.

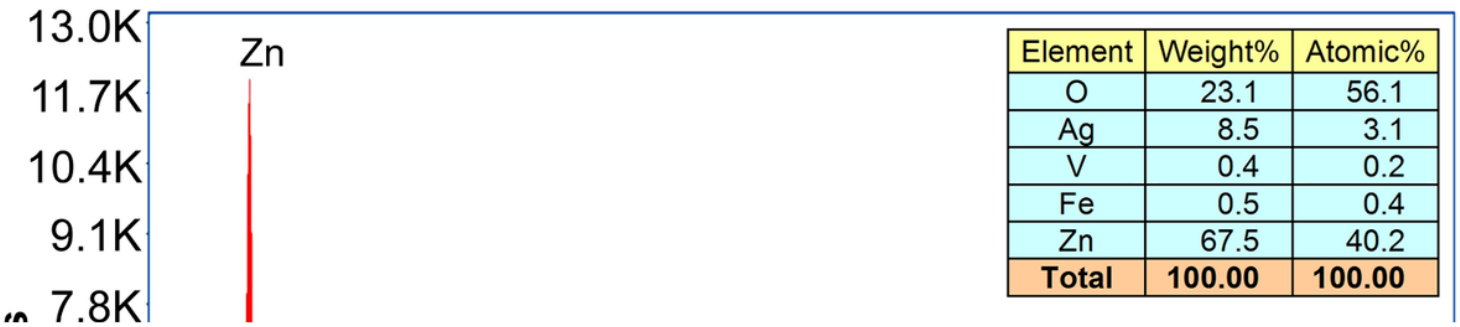

Element	Weight%	Atomic%
O	23.1	56.1
Ag	8.5	3.1
V	0.4	0.2
Fe	0.5	0.4
Zn	67.5	40.2
Total	**100.00**	**100.00**

Figure 5

EDX of 2 wt% Ag-ZnO/$Fe_2V_4O_{13}$.

Figure 6

Elemental color mapping images of 2 wt% Ag-ZnO/$Fe_2V_4O_{13}$: a) 2 wt% Ag-ZnO/$Fe_2V_4O_{13}$ composition, b) O, c) Ag, d) V, e) Fe and f) Zn.

Figure 7

HR-TEM images of 2 wt% Ag-ZnO/$Fe_2V_4O_{13}$: a) 100 nm, b) 50 nm, c) 20 nm, d) 2 nm, e) SAED pattern and f) particle size distribution.

Figure 8

a) UV-DRS and B) K.M plot of a) ZnO, b) $Fe_2V_4O_{13}$, c) 1 wt% Ag-ZnO/$Fe_2V_4O_{13}$, d) 1.5 wt% Ag-ZnO/$Fe_2V_4O_{13}$, e) 2 wt% Ag-ZnO/$Fe_2V_4O_{13}$ and f) 2.5 wt% Ag-ZnO/$Fe_2V_4O_{13}$.

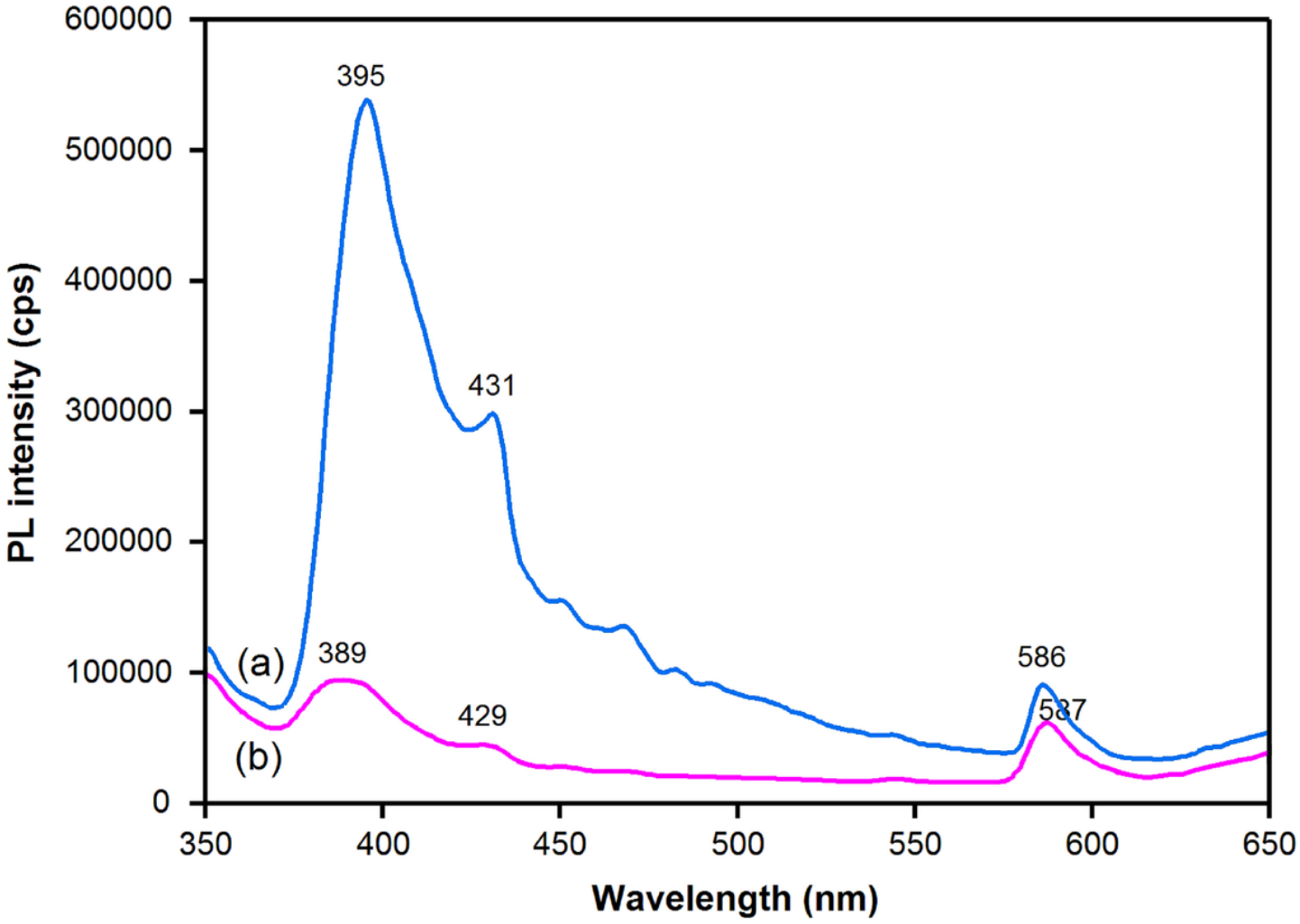

Figure 9

PL spectra of a) ZnO and b) 2 wt% Ag-ZnO/$Fe_2V_4O_{13}$.

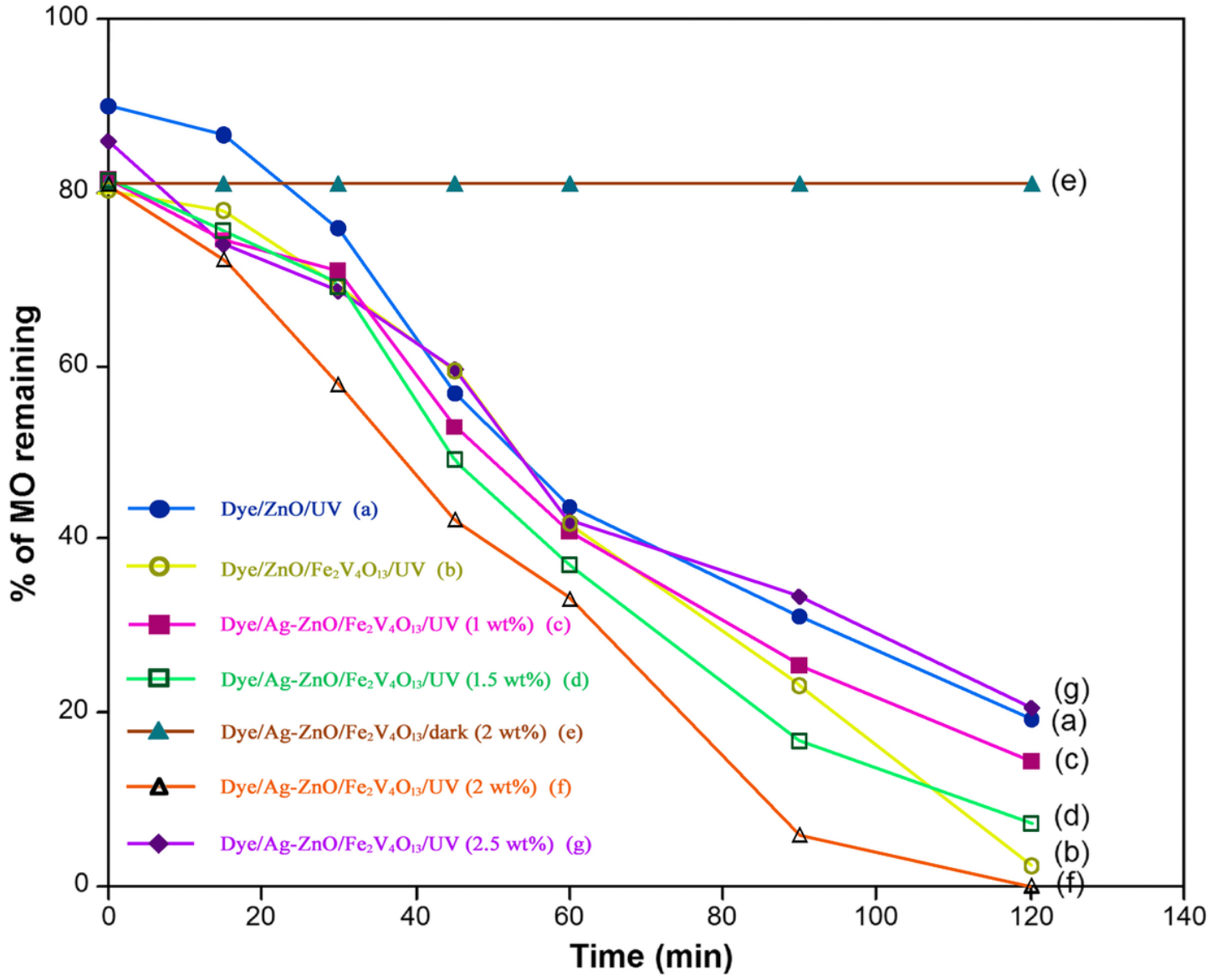

Figure 10

Primary analysis of Ag-ZnO/$Fe_2V_4O_{13}$ catalyst with MO under UV-A light. [MO] = 4 ´ 10^{-4} M, 2 wt% Ag-ZnO/$Fe_2V_4O_{13}$ = 2 g L^{-1}, airflow rate = 8.1 mL s^{-1}, pH = 7.0, I_{UV} = 1.381 ´ 10^{-6} einstein L^{-1} s^{-1}.

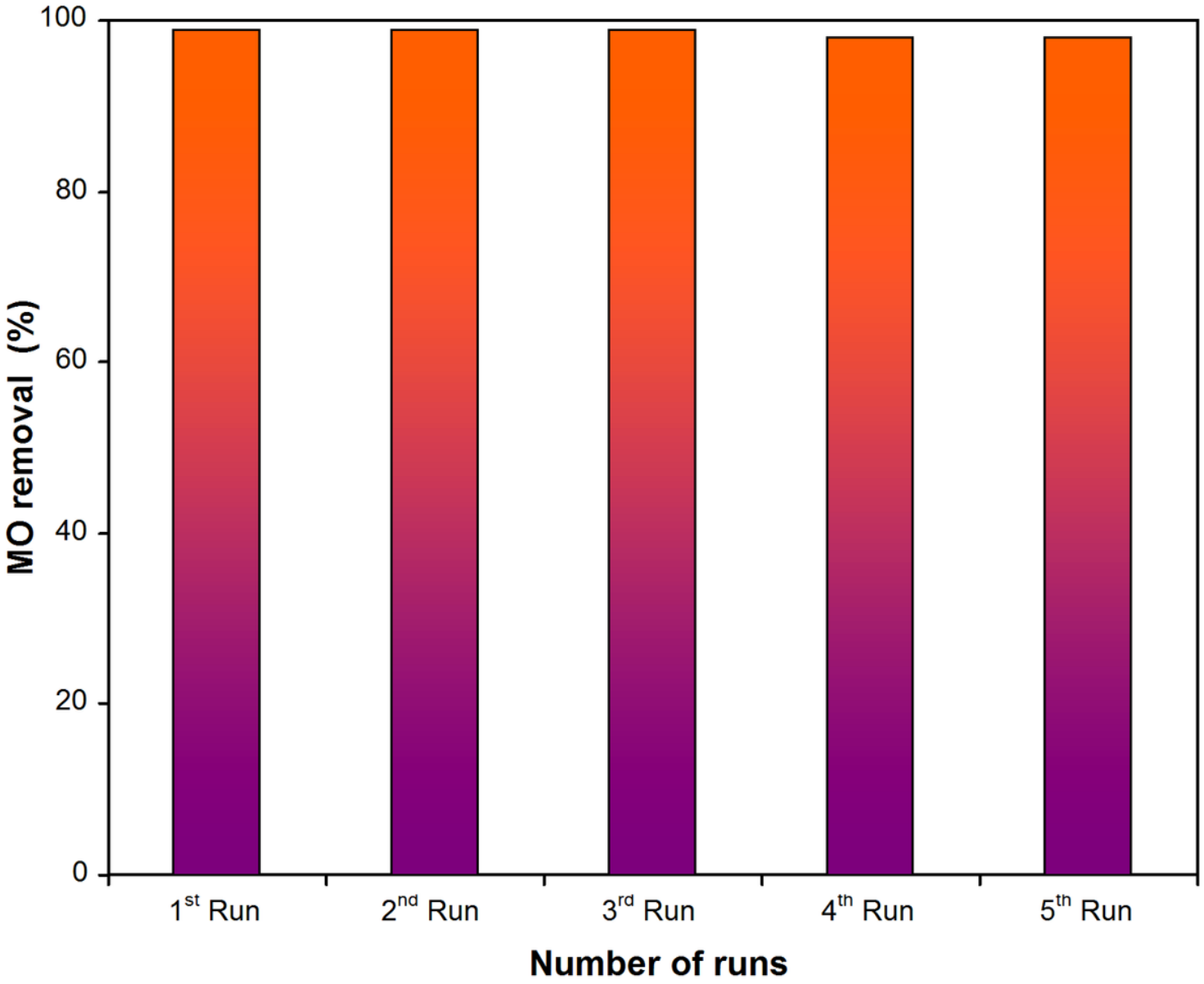

Figure 11

Reusability. [MO] = 4 ´ 10^{-4} M, 2 wt% Ag-ZnO/$Fe_2V_4O_{13}$ = 3 g L^{-1}, airflow rate = 8.1 mL s^{-1}, pH = 7.0, irradiation time = 90 min, I_{UV} = 1.381 ´ 10^{-6} einstein L^{-1} s^{-1}.

Figure 12

Overlay spectrum of MO. [MO] = 4 ´ 10–4 M, 2 wt% Ag-ZnO/$Fe_2V_4O_{13}$ = 3 g L–1, pH = 7.0. a) 0 min, b) 15 min, c) 30 min, d) 45 min, e) 60 min, and f) 90 min

Figure 13

Schematic representation of Ag-ZnO/$Fe_2V_4O_{13}$ nanocomposite mechanism of dye degradation.

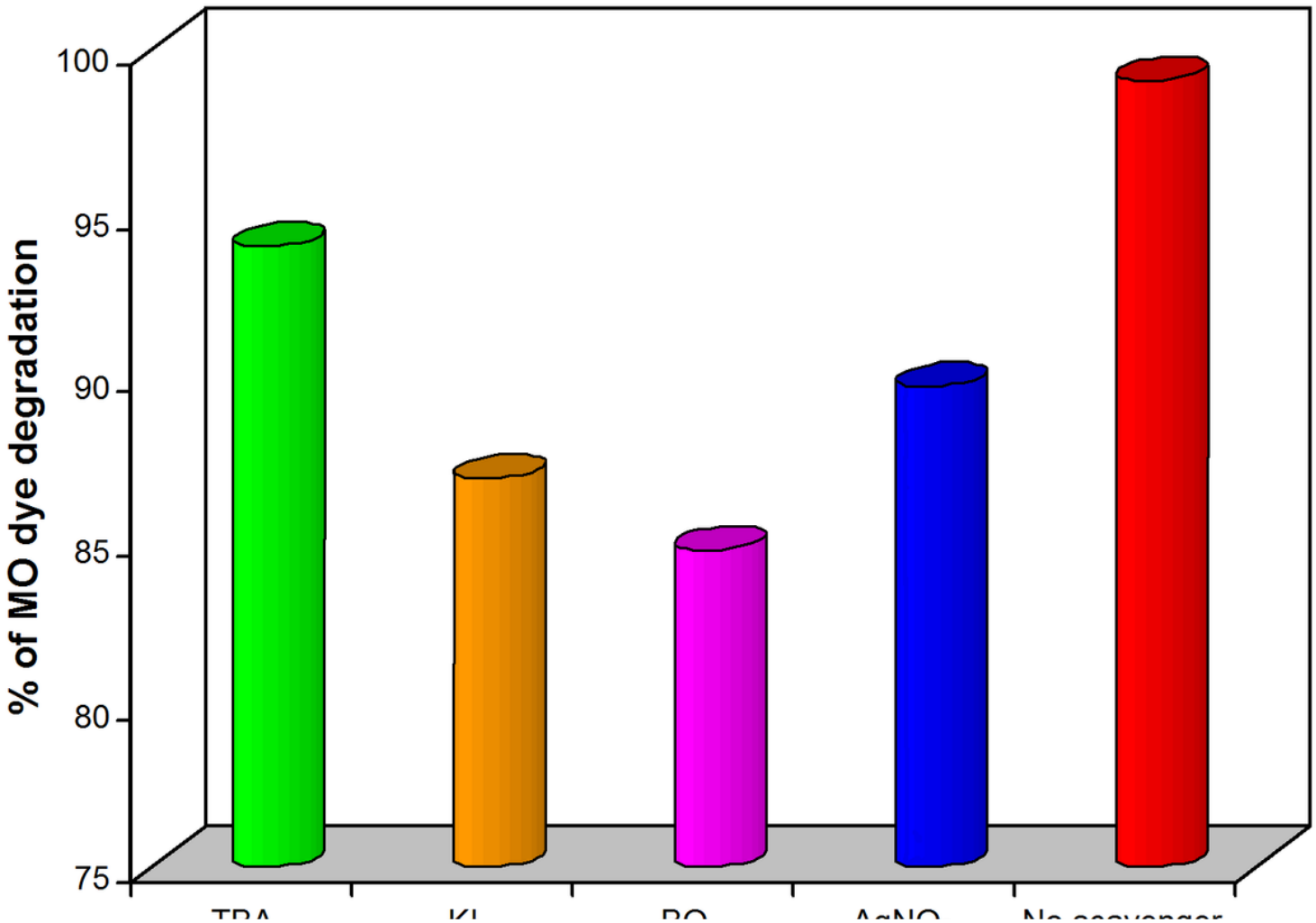

Figure 14

Effect of different scavengers on MO degradation with Ag-ZnO/$Fe_2V_4O_{13}$

Supplementary Files

This is a list of supplementary files associated with this preprint. Click to download.

- 04Supplementarymaterial.doc
- GraphicalAbstract.doc
- Scheme01.png